Available online at www.sciencedirect.com
ScienceDirect
Trans. Nonferrous Met. Soc. China 33(2023) 1851−1861
Transactions of Nonferrous Metals Society of China
www.tnmsc.cn

Effect of alloying elements on thermoelastic properties of Pt-based alloys

Wei YU[1], Xiao-yu CHONG[1], Meng-di GAN[1], Yan WEI[2], Ai-min ZHANG[2], Chang-yi HU[2], Jing FENG[1]

1. Faculty of Materials Science and Engineering, Kunming University of Science and Technology, Kunming 650093, China;
2. Sino-Precious Metals Holding Co., Ltd., Kunming 650106, China

Received 11 January 2022; accepted 30 May 2022

Abstract: Quasi-static approximation based on first-principles calculations was adopted to explore the effect of 33 alloying elements on the thermoelastic properties of Pt-based alloys. The elastic constants and moduli of Pt-based alloy $Pt_{31}X$ were generally lower when rare earth elements (RE=Y, La, Ce, or Th) were dissolved in the Pt matrix, mainly attributed to the higher average bond length between RE and Pt. $Pt_{31}X$ with X=Ta, Nb, V, W, or Mo showed lower average bond lengths and stronger electron localizations than pure Pt, resulting in higher Young's moduli. Meanwhile, the temperature coefficients of the moduli for $Pt_{31}X$ (X=Ta, Nb, V, W, and Mo) were lower in the Pt-based alloys because the average bond length increased slowly with the increase of temperature, among which $Pt_{31}W$ showed the lowest value of $-15.82\times10^{-5}\ K^{-1}$. Therefore, W, Ta, Mo, Nb, or V are considered as the candidate alloying elements for improving the elastic stability.

Key words: first-principles calculation; thermal properties; elastic properties; quasi-static approximation; Pt-based alloy

1 Introduction

The components of precise equipment serving under high temperatures, such as jet nozzles and tension springs, require chemical stability and stable elasticity, i.e., low temperature coefficient of Young's modulus. In addition to being used as catalysts, Pt-based alloys are also widely used as elastic materials owing to their excellent comprehensive properties, such as high melting point, outstanding oxidation resistance, and high corrosion resistance. They are used to manufacture high-precision components and are suitable for various complex (high-temperature, corrosive, or oxidative) environments [1−3]. However, the strength of pure Pt is lower at finite temperatures, and the elastic heat resistance of Pt-based alloys must be further improved by alloying [1,4−6]. The high-temperature strength and creep resistance of Pt are significantly improved by adding Rh, forming alloys such as Pt−7Rh and Pt−10Rh [7]. At the same time, dissolving a small amount of alloying elements (Mo, W, Ru, and Ir) in Pt−Rh alloys increases the endurance strength and reduces the creep rate [8]. Moreover, the high-temperature strength and creep resistance of Pt are also promoted when small amounts of Zr and Y are dissolved into the Pt matrix [9]. The commonly used Pt-based alloys are Pt−Rh [7,8], Pt−Ir [3,10], and Pt−Zr [11,12]. However, the experimental investigation of each alloy is very expensive and ineffective. First-principles calculation based on density functional theory (DFT) is a convenient and efficient way to understand and predict the properties of materials, which has already been successfully applied in the investigation of Pt−Al [13,14] and Pt−Sc [15−17]. In our previous

Corresponding author: Xiao-yu CHONG, E-mail: xiaoyuchong@kust.edu.cn;
Yan WEI, E-mail: weiyan@ipm.com.cn
DOI: 10.1016/S1003-6326(23)66227-2

work, the effects of 33 alloying elements on the elastic properties of Pt-based dilute alloys were studied systematically using first-principles calculations at 0 K. It was found that $Pt_{31}W$, $Pt_{31}Mo$, $Pt_{31}Nb$, and $Pt_{31}V$ have higher Young's moduli. However, the performance of Pt-based alloys in complex service environments, e.g., at high temperatures, is still unclear. Based on our previous research, in the present study, the thermoelastic properties of Pt-based dilute alloys were estimated using quasi-static approximation (QSA) combined with first-principles calculations. At the same time, the thermodynamic properties from first-principles calculations, e.g., enthalpy, entropy, and heat capacity, could also be used to construct thermodynamic models of Pt-based alloys in the future.

2 Theory and method

The thermodynamic properties of Pt-based dilute alloys at finite temperatures are obtained using the quasiharmonic approach (QHA) [18,19]. The Helmholtz free energy $F(V, T)$ at volume V and temperature T is given by [20]

$$F(V,T)=E_{\mathrm{c}}(V)+F_{\mathrm{el}}(V,T)+F_{\mathrm{vib}}(V,T) \tag{1}$$

where $E_{\mathrm{c}}(V)$ is the static total energy at 0 K without zero-point vibrational energy, estimated using the following five-parameter modified Brich–Murnaghan equation of state (mBM-EOS) [21]:

$$E_{\mathrm{c}}(V)=a+bV^{-1/3}+cV^{-2/3}+dV^{-3/3}+eV^{-4/3} \tag{2}$$

where a, b, c, d, and e are constants. Seven first-principles energy versus volume data points in the range of 0.97−1.03 times the lattice constants were employed in this work.

$F_{\mathrm{el}}(V, T)$ in Eq. (1) is the Helmholtz free energy from the thermal electronic contribution, determined by the Mermin statistics: $F_{\mathrm{el}}(V, T)=E_{\mathrm{el}}-TS_{\mathrm{el}}$, where E_{el} is the internal energy and S_{el} is the bare electronic entropy. The internal energy owing to electronic excitations at volume V and temperature T is expressed by [20]

$$E_{\mathrm{el}}(V,T)=\int n(\varepsilon,V)f\varepsilon\mathrm{d}\varepsilon-\int n(\varepsilon,V)\varepsilon\mathrm{d}\varepsilon \tag{3}$$

The bare electronic entropy caused by electronic excitation is given by

$$S_{\mathrm{el}}(V,T)=-k_{\mathrm{B}}\int n(\varepsilon,V)[f\ln f+(1-f)\ln(1-f)]\mathrm{d}\varepsilon \tag{4}$$

where $n(\varepsilon, V)$, ε, f, and k_{B} are the electronic density of state, energy eigenvalue, Fermi distribution function, and Boltzmann constant, respectively.

$F_{\mathrm{vib}}(V, T)$ in Eq. (1) is the Helmholtz free energy from the vibrational contribution. Based on the frequency (ω) distribution, it is expressed as follows [20]:

$$F_{\mathrm{vib}}(V,T)=k_{\mathrm{B}}T\sum_{q}\sum_{j}\ln\left\{2\sinh\left[\frac{\hbar\omega_j(q,V)}{2k_{\mathrm{B}}T}\right]\right\} \tag{5}$$

where q is the amplitude of the wave vector, j is the jth phonon mode, and $\hbar$ is the reduced Planck constant.

Meanwhile, the Helmholtz free energy from the vibrational contribution can also be predicted using the Debye–Grüneisen model [18,22]:

$$F_{\mathrm{vib}}(V,T)=\frac{9}{8}k_{\mathrm{B}}\Theta_{\mathrm{D}}+k_{\mathrm{B}}T\left\{3\ln\left[1-\exp\left(-\frac{\Theta_{\mathrm{D}}}{T}\right)\right]-D\left(\frac{\Theta_{\mathrm{D}}}{T}\right)\right\} \tag{6}$$

where Θ_{D} is the Debye temperature, and $D(x)$ is the Debye function given by

$$D(y)=\frac{3}{y^3}\int_0^y\frac{t^3}{\exp t-1}\mathrm{d}t \tag{7}$$

where y is Θ_{D}/T, and t is a variable.

The Debye temperature can be obtained using the Debye–Grüneisen model as follows [22]:

$$\Theta_{\mathrm{D}}=sAV_0^{1/6}\left(\frac{B_0}{M}\right)^{1/2}\left(\frac{V_0}{V}\right)^{\gamma} \tag{8}$$

where s (=0.617) is a scaling factor obtained by MORUZZI et al [22]; V_0 is equilibrium volume; γ is the Grüneisen constant defined by $\gamma=\left(\frac{1+B_0}{2}-x\right)$, B_0 is the bulk modulus and x is a constant related to the solvent; A and M are a constant and average relative atomic mass, respectively.

The bulk modulus (B) and shear modulus (G) of Pt were obtained using the Voigt–Reuss–Hill (VRH) laws, and Young's modulus (E) was obtained using Eq. (9) [23,24]:

$$E=\frac{9BG}{3B+G} \tag{9}$$

First-principles calculations were performed as implemented in the DFTTK high-throughput software [25] based on the Vienna ab initio

simulation package (VASP) [26]. The thermoelastic properties were estimated according to the property–volume relationship from the QHA and QSA approaches. The exchange–correction functional was computed using Perdew−Burke−Ernzerh for solids (PBEsol) of generalized gradient approximation (GGA) with projector augmented-wave (PAW) pseudopotential [27]. The $20 \times 20 \times 20$ and $10 \times 10 \times 10$ k-point sampling meshes were employed for the unit cells of Pt (4 atoms) and $Pt_{31}X$ (32 atoms), respectively, based on the Monkhorst–Pack scheme [26]. The energy cutoff of the wave function of 400 eV was used, and the energy convergence criterion for self-consistency was 1×10^{-8} eV/atom. Considering the estimation of Helmholtz free energy from the vibrational contribution by the phonon model, the supercell approach based on the density functional perturbation theory (DFPT) was used with a $2 \times 2 \times 2$ supercell of the conventional unit cell of Pt as implemented in the phonopy code [28]. The high-throughput workflow for screening candidate alloying elements is shown in Fig. 1; more details of the first-principles calculations can be found in our previous works [17,24].

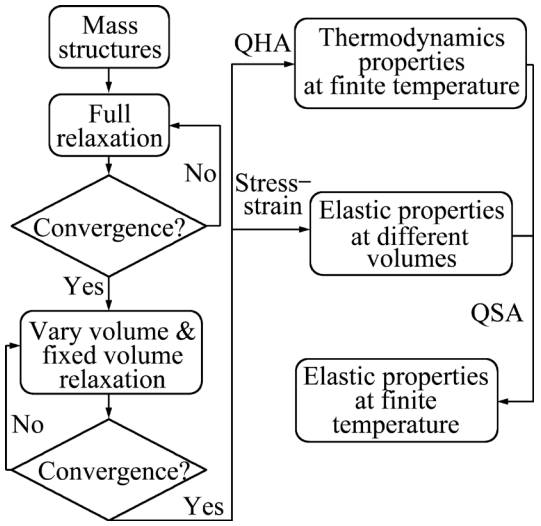

Fig. 1 High-throughput workflow for screening candidate alloying elements

3 Results and discussion

3.1 Thermoelastic properties of Pt

Pt is a face-centered cubic metal (Fig. 2(a)) that belongs to $Fm\bar{3}m$ space group (No. 225) [17]. The energy vs volume data points for Pt were fitted

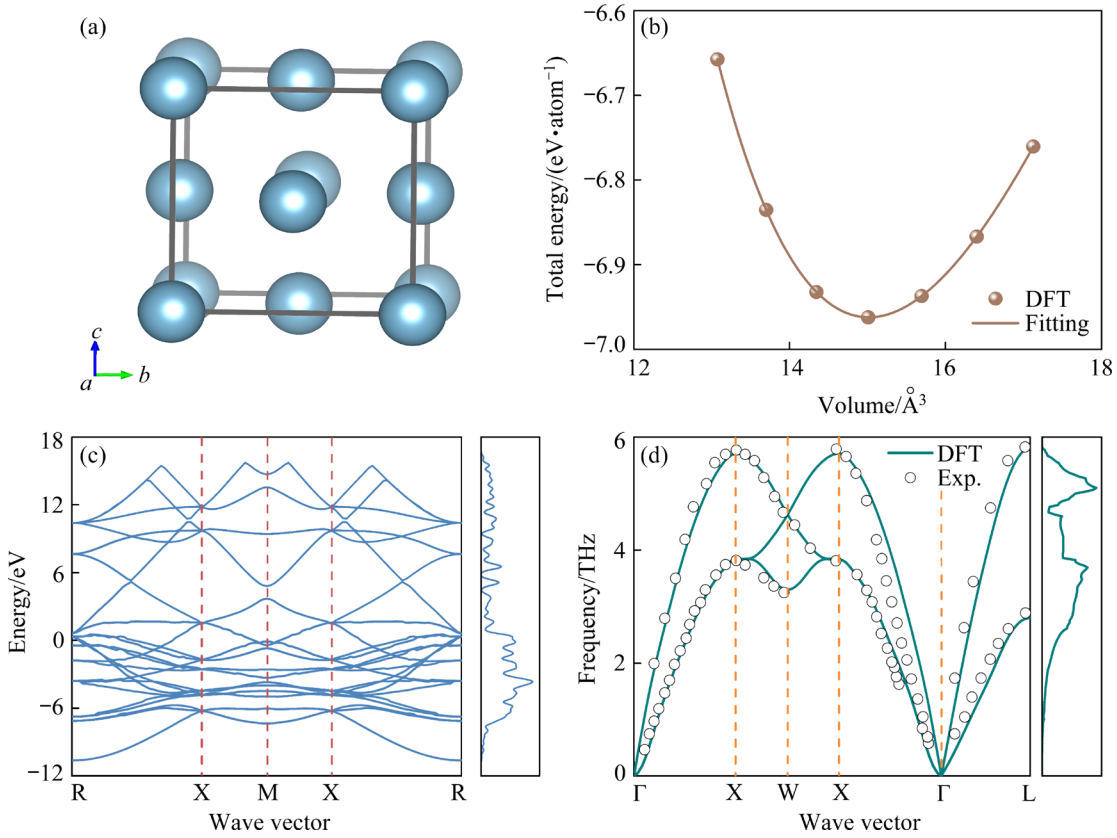

Fig. 2 Crystal structure of Pt (a), energy as function of volume of per unit Pt atom (b), electronic band structure and density of state of Pt (c) and phonon dispersions and phonon density of state of Pt (d)

according to a five-parameter mBM-EOS, as shown in Fig. 2(b). The results are shown in Table S1 in Supplementary Materials and are consistent with published experimental data and results of other works [29−31]. Smaller equilibrium volume is attributed to the experimental value being measured at room temperature. The electronic band structure and density of state of Pt at the theoretical equilibrium volume are shown in Fig. 2(c). The Helmholtz free energy from the thermal electronic contribution cannot be ignored at finite temperatures owing to non-zero densities around the Fermi level, predicted via integration over the electronic density of state [20]. In addition, there are phonon dispersion curves of Pt at the theoretical equilibrium volume together with room temperature measurements by neutron diffraction [32] in Fig. 2(d), and the calculated values agree well with the experimental ones. The Helmholtz free energy from the vibrational contribution was estimated based on the results of phonon calculations. Moreover, for simplicity, because many structures were needed to be treated, the vibrational contribution to the Helmholtz free energy was also obtained using the Debye–Grüneisen model. Notably, the thermodynamic properties of Pt from the Debye–Grüneisen model require adjusting the appropriate parameter (x) in Eq. (7) [18,20]; thus, x was examined in this study.

Figures 3(a–d) show the entropy, enthalpy, specific heat capacity, and linear thermal expansion coefficients (LTEC) of Pt from the phonon and Debye–Grüneisen models, along with the experimental value. The enthalpy of Pt from the phonon and Debye–Grüneisen models was estimated using $H=F+TS$ (H is the enthalpy, F is the Helmholtz free energy, and S is the entropy); moreover, the reference state was commonly used, i.e., H at 298.15 K and 1.013×10^5 Pa. The thermodynamic properties of Pt, including entropy, enthalpy, specific heat capacity, and LTEC gradually decrease with the increase in parameter x, mainly attributed to the decrease in Grüneisen constants with the increase in parameter x, weakening the anharmonic effect. Entropy and enthalpy of Pt from the Debye–Grüneisen and phonon models were in good agreement with the recommended values [33,34]. Moreover, entropy and enthalpy of Pt from the Debye–Grüneisen model were more accurate than those from the

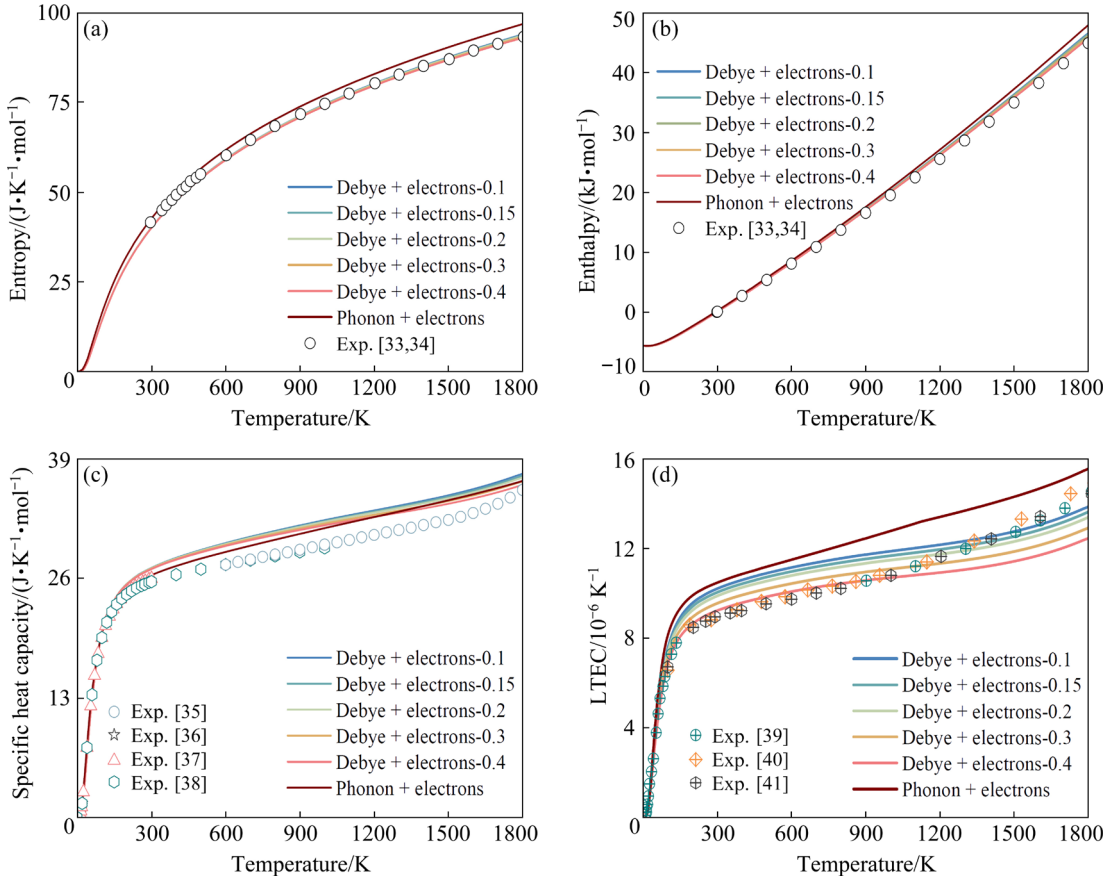

Fig. 3 Thermal properties of Pt: (a) Entropy; (b) Enthalpy; (c) Specific heat capacity; (d) LTEC

phonon model at high temperatures in the present study. At the same time, specific heat capacity from the phonon and Debye−Grüneisen models agreed well with the recommended values [35−38].

With the change in parameter x, the entropy, enthalpy, and specific heat capacity of Pt showed no significant changes; however, LTECs depended heavily on the selected parameter x. Figure 3(d) shows LTECs of Pt, along with the experimental values. Notably, the LTECs of Pt from phonons and the Debye–Grüneisen models are in extremely good agreement with experimental values [39]. In addition, Fig. S1 in Supplementary Materials (SM) shows the error of the LTECs between the calculated and experimental values [40]. The low-temperature error of LTECs from the Debye–Grüneisen model decreases steadily with an increase in parameter x, but the relationship is reversed at high temperatures. The error of the LTECs from the phonon model decreases with an increase in temperature. Meanwhile, the volume of pure Pt exhibits favorable agreement with experimental values in Fig. S2 in SM and hot electrons significantly contribute to the thermo-dynamic properties in Fig. S3 in SM. Overall, the thermo-dynamic properties of Pt were predicted by the Debye–Grüneisen model.

The temperature-dependent elastic properties were estimated through an efficient QSA, which was adopted because the changes in elastic properties are mainly controlled by the volume change and anharmonic effect, and the contributions of kinetic energy and fluctuation of microscopic stress tensors are ignored [18,20]. The elastic constants of Pt (C_{11}, C_{12}, and C_{44}) at different volumes were estimated using the stress–strain method [24]. Figure 4(a) summarizes the temperature-dependent elastic constants, which agree well with the experimental values. The elastic constants decrease with increasing temperature. Furthermore, the elastic properties of polycrystalline materials were obtained using the VRH laws [17,24]. Figure 4(b) shows the elastic moduli of Pt (B, G, and E), which agree well with the experimental values, especially G and E, indicating that the selected approach can capture the high-temperature elastic properties of Pt-based dilute alloys.

3.2 Thermoelastic properties of Pt-based alloys

The static total energy of the Pt-based alloys (Table S1 in SM) was calculated using the mBM-

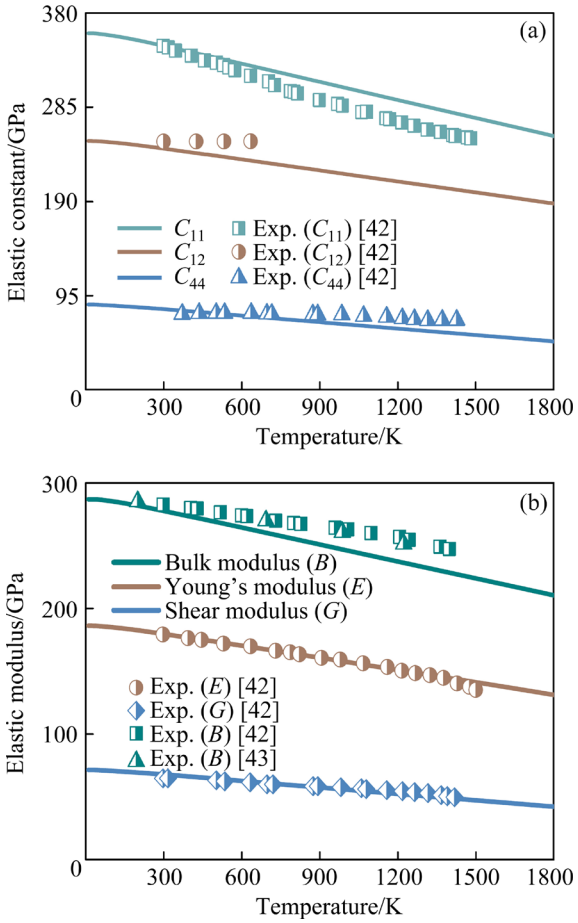

Fig. 4 Temperature-dependent elastic constants (a) and elastic moduli (b) of Pt, including C_{11}, C_{12}, C_{44}, B, G, and E

EOS results in Fig. 5(a). Then, the thermodynamic properties of Pt-based alloys were estimated by QHA combined with the Debye–Grüneisen model. The entropy, enthalpy, and volume of Pt-based alloys with thermal electronic contributions at finite temperatures are shown in Figs. 5(b–d), respectively. The stability of the system is affected by entropy, i.e., a larger entropy improves the stability of Pt-based alloys, such as $Pt_{31}Pd$, $Pt_{31}Rh$, $Pt_{31}Ir$, and $Pt_{31}Au$, especially at finite temperatures. In addition, the volume of Pt-based alloys increases with the increase of temperature, with the volume increase correlated with the atomic radius of the alloying element dissolved in the Pt matrix, i.e., it was larger in the cases of Th, La, Ce, Y, Zr, Hf, and Sc, and vice versa for elements with smaller radii.

The temperature-dependent elastic properties of Pt-based alloys, including C_{11}, C_{12}, C_{44}, B, G, and E, predicted based on the QSA are shown in Figs. 6(a–f), respectively. Meanwhile, the fitting parameters of elastic constants are listed in Table S2

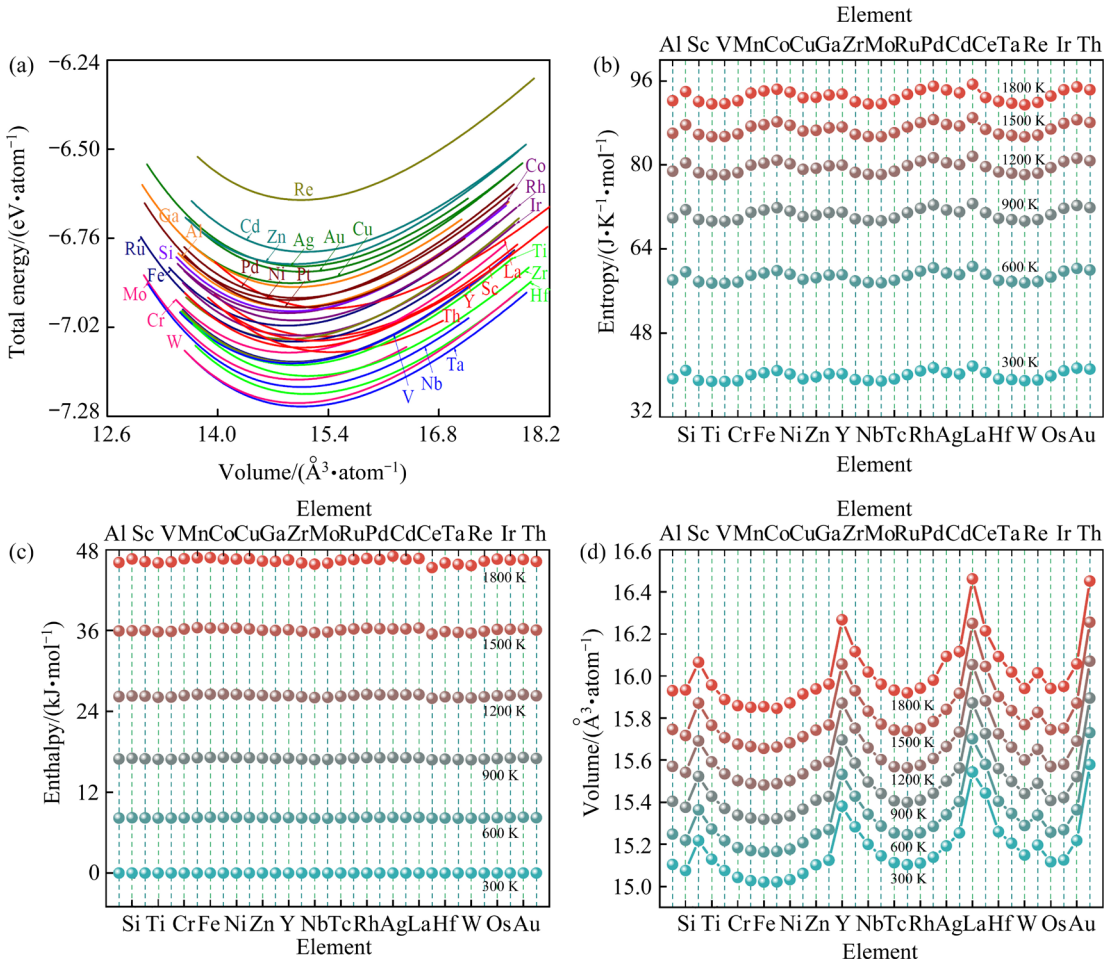

Fig. 5 Thermal properties of Pt-based alloys: (a) Energy as function of volume; (b) Entropy; (c) Enthalpy; (d) Volume

in SM. Elastic constants and elastic moduli gradually decrease with increasing temperature. The C_{11} was smaller in alloys with rare earth elements (Y, La, Ce, and Th), leading to a smaller B. In addition, the moduli of $Pt_{31}RE$ were generally lower, partly owing to the large atomic radii of rare earth elements. The larger C_{44} of $Pt_{31}W$, $Pt_{31}Ta$, $Pt_{31}Mo$, and $Pt_{31}Nb$ led to higher G. Moreover, $Pt_{31}W$, $Pt_{31}Ta$, $Pt_{31}Mo$, $Pt_{31}Nb$, and $Pt_{31}V$ showed larger E, consistent with the results of our previous work [17].

Figure S4 in SM shows the Debye temperatures of the Pt-based dilute alloys. The Debye temperature corresponds to the highest frequency of lattice vibration and reflects the strength of the chemical bond, i.e., the higher the Debye temperature, the larger the E [30]. The calculated Debye temperature of Pt was 250 K, and its experimental value is 240 K [30]. $Pt_{31}W$, $Pt_{31}Ta$, $Pt_{31}Mo$, $Pt_{31}Nb$, and $Pt_{31}V$ had higher Debye temperatures, while the Debye temperatures of $Pt_{31}Rh$, $Pt_{31}Pd$, $Pt_{31}Au$, $Pt_{31}La$, $Pt_{31}Ce$, and $Pt_{31}Th$ were lower. $Pt_{31}V$ showed the highest Debye temperature (263.61 K), whereas that of $Pt_{31}La$ (234.79 K) was the lowest, which were consistent with the results of previous analysis.

3.3 Temperature coefficient of Pt-based alloys

Interestingly, $Pt_{31}X$ (X=Ta, Nb, V, W, and Mo) exhibited high G and E, and high normalized elastic moduli (Figs. 6(e, f)), i.e., the elastic moduli decreased at a low rate with increasing temperature, resulting in high durable strength. Then, the elastic heat resistance was evaluated by the rate of change of the elastic modulus with temperature, estimated by the temperature sensitivity coefficient (λ) and temperature coefficient of $E(\beta)$. The former is defined as follows:

$$\lambda = \Delta M / \Delta T \tag{10}$$

where ΔM and ΔT are the changes in the elastic modulus (B, G, and E) and temperature, respectively. When ΔM=ΔE, the temperature coefficient of E is calculated as

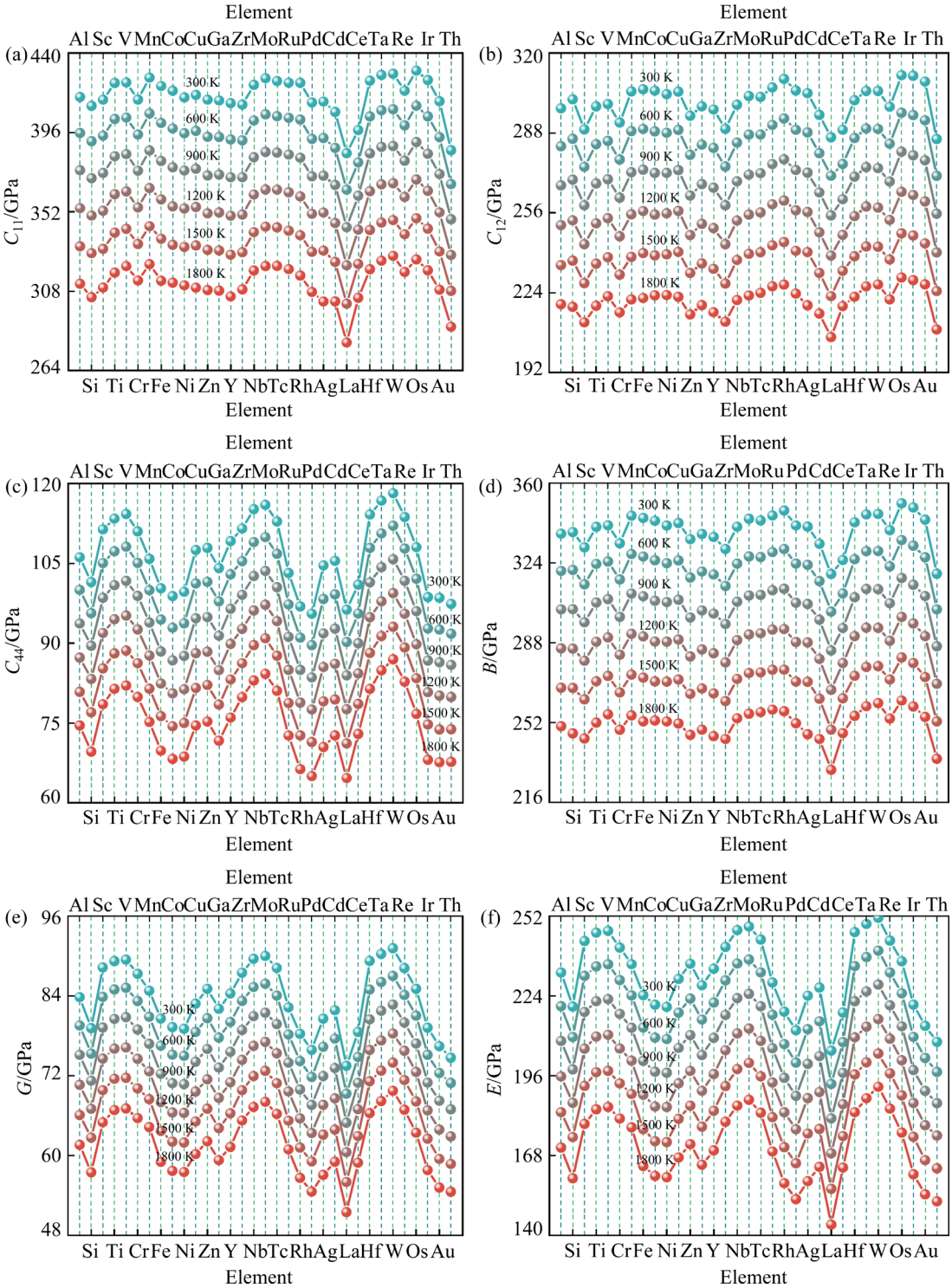

Fig. 6 Temperature-dependent elastic properties of Pt-based alloys: (a) C_{11}; (b) C_{12}; (c) C_{44}, (d) B; (e) G; (f) E

$$\beta = \lambda / E_0 \tag{11}$$

where E_0 is Young's modulus at 273.15 K. The temperature sensitivity coefficients of the Pt-based dilute alloys are listed in Fig. S5 in SM (the negative values indicate that the modulus decreases gradually with an increase in temperature). The temperature sensitivity coefficient of the elastic modulus of Pt was predicted using experimental and calculated values. Temperature sensitivity coefficients of B, G, and E estimated by experimental value were −0.0307, −0.0126, and −0.0346 GPa/K, respectively, while those predicted from the calculated value in this work were −0.0388, −0.0171, and −0.0324 GPa/K, respectively, indicating that this method is accurate and reliable.

The temperature sensitivity coefficient of B has larger absolute values in alloys with elements from IB, VIIB, and VIII groups. In addition, the temperature sensitivity coefficients of G and E have higher absolute values in Pt-based alloys with alloying elements from both ends of the periodic table. The temperature coefficients of E predicted using Eq. (11) are shown in Fig. 7. The temperature coefficient of E for Pt estimated from the experimental value was $-19.28\times10^{-5}\,K^{-1}$, and that predicted from the calculated value in this work was $-18.13\times10^{-5}\,K^{-1}$. The absolute value of the temperature coefficient of E for Pt-based alloys firstly decreased and then increased with an increase in the atomic number for alloying elements from the same period.

The absolute value of the temperature coefficient of E was smaller for the alloying elements from VB, VIB, and VIIB groups. Particularly, $Pt_{31}W$, $Pt_{31}Ta$, $Pt_{31}Mo$, $Pt_{31}Nb$, $Pt_{31}V$, $Pt_{31}Cr$, $Pt_{31}Re$, $Pt_{31}Mn$, and $Pt_{31}Ti$ all showed lower values of the temperature coefficient of E, among which $Pt_{31}W$ exhibited the lowest value ($-15.82\times10^{-5}\,K^{-1}$).

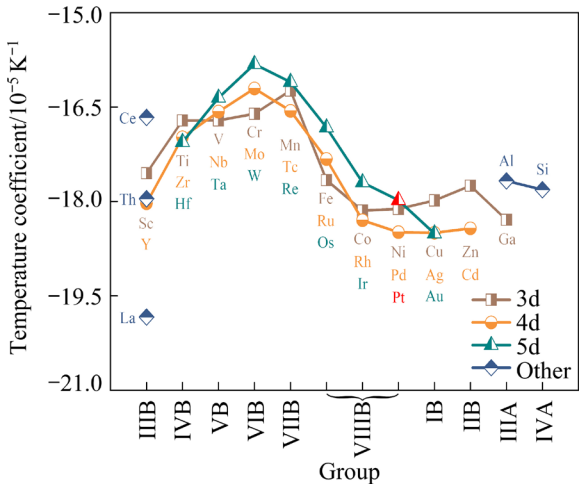

Fig. 7 Temperature coefficients of E for Pt-based alloys

3.4 Electronic structure of Pt-based alloys

Finally, the local chemical bonds of the Pt-based alloys were analyzed. The average bond lengths of Pt—Pt and Pt—X bonds (X represents the 33 alloying elements) are shown in Figs. 8(a) and (b), respectively. The fitting parameters of bond length are listed in Table S3 in SM. The bond length and elastic properties show opposite trends, i.e, the change of the elastic properties with atomic number presents a downward opening parabola, and the bond length is upward opening. The average lengths of Pt—Pt and Pt—X bonds gradually increased with increasing temperature. The average lengths of Pt—Pt and Pt—X bonds (X=Y, La, Ce, and Th) were larger in the alloys. $Pt_{31}Th$ showed the highest average Pt—Pt bond length, and $Pt_{31}La$ exhibited the highest average Pt—X bond length. For this reason, $Pt_{31}La$ showed the lowest elastic moduli (B, G, and E) and Debye temperature.

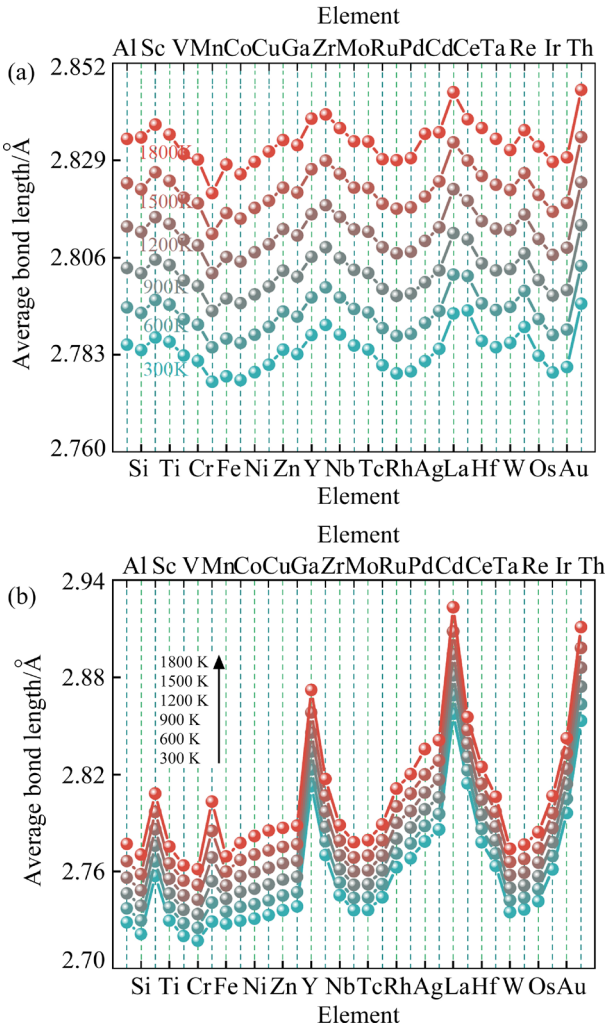

Fig. 8 Average lengths of Pt—Pt (a) and Pt—X (b) bonds

When alloying elements (X=Cr, V, Ti, W, Re, Mo, and Tc) were introduced into the Pt matrix, the average bond length in Pt—X was lower than that in pure Pt even at 1800 K, especially for Cr and V. Therefore, $Pt_{31}Cr$, $Pt_{31}V$, $Pt_{31}Ti$, $Pt_{31}W$, $Pt_{31}Re$, $Pt_{31}Mo$, and $Pt_{31}Tc$ showed higher elastic moduli and Debye temperatures. Meanwhile, the average bond length of the Pt—Pt bonds did not change significantly after different alloying elements were introduced into the Pt matrix, meaning that Pt—X bonds played a dominant role.

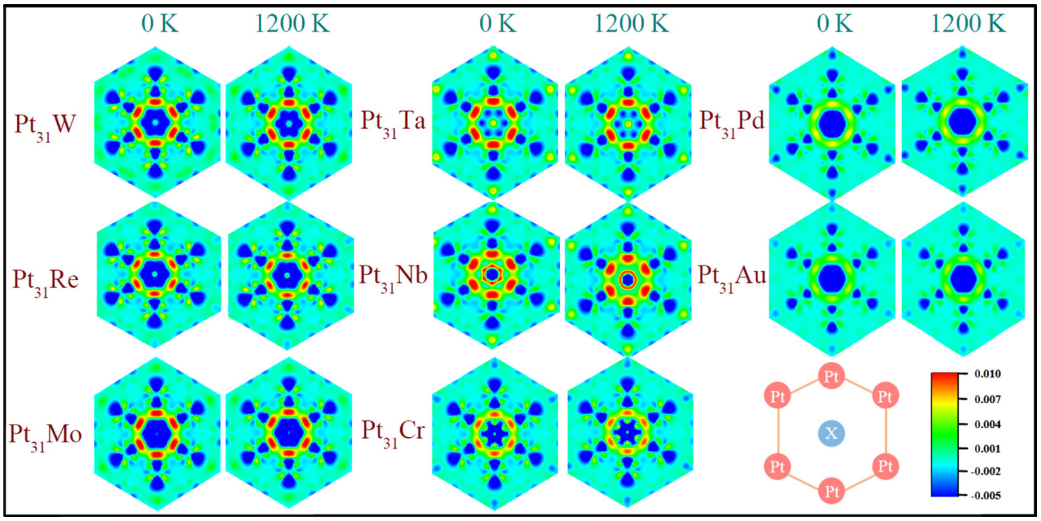

Fig. 9 Charge density differences of (111) plane in Pt-based dilute alloys at different temperatures, including $Pt_{31}W$, $Pt_{31}Re$, $Pt_{31}Mo$, $Pt_{31}Ta$, $Pt_{31}Nb$, $Pt_{31}Cr$, $Pt_{31}Pd$, and $Pt_{31}Au$

Several typical Pt-based alloys, including those with small temperature coefficients ($Pt_{31}W$, $Pt_{31}Re$, $Pt_{31}Mo$, $Pt_{31}Ta$, $Pt_{31}Nb$, and $Pt_{31}Cr$) and large temperature coefficients ($Pt_{31}Pd$ and $Pt_{31}Au$), were selected to analyze their charge density difference (CDD). Sorted by the absolute value of the temperature coefficient of E in ascending order, these alloys come in the following order: $Pt_{31}W$ < $Pt_{31}Re$ < $Pt_{31}Mo$ < $Pt_{31}Ta$ < $Pt_{31}Nb$ < $Pt_{31}Cr$ < $Pt_{31}Pd$ < $Pt_{31}Au$.

Figure 9 shows the CDD of the (111) plane of Pt-based alloys at 0 and 1200 K. The results show that the degree of electron localization in Pt-based alloys decreases gradually in $Pt_{31}W$, $Pt_{31}Re$, $Pt_{31}Mo$, $Pt_{31}Ta$, $Pt_{31}Nb$, $Pt_{31}Cr$, $Pt_{31}Pd$, and $Pt_{31}Au$ at 0 K. Meanwhile, the degree of electron localization at 1200 K is lower than that at 0 K. The increased degree of electron non-localization at 1200 K weakens the interaction between atoms, consistent with the above results that the bond length increases with increasing temperature. In addition, electron clouds tend to be nonspherical in $Pt_{31}W$, $Pt_{31}Re$, $Pt_{31}Mo$, $Pt_{31}Ta$, $Pt_{31}Nb$, and $Pt_{31}Cr$, which is beneficial to improving the elastic modulus, reducing the temperature coefficient of E, and enhancing the elastic heat resistance of Pt-based dilute alloys.

4 Conclusions

(1) The thermodynamic properties of Pt were well predicted by the Debye–Grüneisen model.

(2) The alloys with rare-earth elements (RE=Y, La, Ce, and Th) showed lower elastic moduli and Debye temperatures. The analysis of local chemical bonds showed that these alloys generally showed higher average lengths of Pt—Pt and Pt—RE bonds. $Pt_{31}Th$ exhibited the highest average Pt—Pt bond length, and $Pt_{31}La$ showed the highest average Pt—RE bond length.

(3) $Pt_{31}W$, $Pt_{31}Ta$, $Pt_{31}Mo$, $Pt_{31}Nb$, and $Pt_{31}V$ showed overall higher elastic moduli and Debye temperatures, attributed to the lower average bond length and stronger electron localization. The electron clouds in these alloys tend to be nonspherical, which improves the elastic modulus.

(4) $Pt_{31}W$, $Pt_{31}Ta$, $Pt_{31}Mo$, $Pt_{31}Nb$, $Pt_{31}V$, $Pt_{31}Cr$, $Pt_{31}Re$, $Pt_{31}Mn$, and $Pt_{31}Ti$ showed lower temperature coefficients of E (with $Pt_{31}W$ showing the lowest value of -15.82×10^{-5} K^{-1}) because their average bond lengths increased slowly with increasing temperature, even at high temperatures. Therefore, W, Ta, Mo, Nb, and V are suggested as candidate alloying elements to strengthen the elastic heat resistance and weaken the temperature dependence of the elastic properties.

Acknowledgments

The authors would like to thank the financial support from the Rare and Precious Metals Material Genetic Engineering Project of Yunnan Province, China (Nos. 202102AB080019-1, 202002AB080001-1), the Yunnan Fundamental

Research Projects, China (Nos. 202101AW070011, 202101BE070001-015), and the Youth Project of Yunnan Basic Research Program, China (No. 202001AU070033).

Supplementary Materials

Supplementary Materials in this paper can be found at: http://tnmsc.csu.edu.cn/download/19-p1851-2021-1639-Supplementary_materials.pdf.

References

[1] YAO Xin, MAO Yong, GUO Ya-fang. First-principles study of the alloying effects on the structural stability and mechanical properties of $L1_2$-Pt3Hf [J]. Journal of Alloys and Compounds, 2022, 891: 161982.

[2] LI Zong-bo, XIONG Kai, JIN Cheng-chen, SUN Ying-jie, WANG Bao-wen, ZHANG Shun-meng, HE Jun-jie, MAO Yong. Structural, mechanical, thermodynamic and electronic properties of Pt_3M (M=Al, Co, Hf, Sc, Y, Zr) compounds under high pressure [J]. Rare Metals, 2021, 40: 1208−1218.

[3] ZHOU Yun-xan, CHONG Xiao-yu, HU Ming-yu, WEI Yu, HU Chang-yi, ZHANG Ai-min, FENG Jing. Probing the mechanical properties of ordered and disordered Pt−Ir alloys by first-principles calculations [J]. Physics Letters A, 2021, 405: 127424.

[4] LIN Gao-yong, LI Kun, FENG Di, FENG Yong-ping, SONG Wei-yuan, XIAO Meng-qiong. Effects of La−Ce addition on microstructure and mechanical properties of Al−18Si−4Cu−0.5Mg alloy [J]. Transactions of Nonferrous Metals Society of China, 2019, 29: 1592−1600.

[5] NAMI B, MIRESMAEILI S M, JAMSHIDI F, KHOUBROU I. Effect of Ca addition on microstructure and impression creep behavior of cast AZ61 magnesium alloy [J]. Transactions of Nonferrous Metals Society of China, 2019, 29: 2056−2065.

[6] ZHANG Wan-peng, MA Ming-long, YUAN Jia-wei, SHI Guo-liang, LI Yon-jun, LI Xing-gang, ZHANG Kui. Microstructure and thermophysical properties of Mg−2Zn−xCu alloys [J]. Transactions of Nonferrous Metals Society of China, 2020, 30: 1803−1815.

[7] TIAN Min, HU Chang-yi, CAI Hong-zhong, LI Xiang, WEI Yan, HE Lian-long. A novel ultra-high temperature Pt−Rh alloy with balanced tensile strength and creep resistance achieved by rare-earth intermetallics [J]. Materials Science and Engineering A, 2020, 797: 139966.

[8] LI Jia-yan, XIE Ming, YANG You-cai, ZHANG Ji-ming, CHEN Yong-tai, LIU Man-men, WANG Sai-bei, HU Jie-qiong, NIN Ping. Effect of Zr, Mo and Y adding on microstructure, mechanical and electrical properties of Au−Pd, Pt−Ir and Pd−Ru systems [J]. Rare Metal Materials and Engineering, 2013, 42: 2027−2033.

[9] ZHANG Qiao-xin, ZHANG Dong-ming, JIA Shi-chong, SHONG Wu-lin. Microstructure and properties of some dispersion strengthened platinum alloys [J]. J Platinum Metals Review, 1995, 39: 167−171.

[10] TSENG S F, LEE C J, HUANG K C, CHIANG D Y, HUANG C Y, CHOU C P. Mechanical properties of Pt−Ir and Ni−Ir binary alloys for glass-molding dies coating [J]. Journal of Nanoscience and Nanotechnology, 2011, 11: 8682−8688.

[11] PAN Yong, LIN Yuan-hua, WANG Xiao-hong, CHEN Song-song, WANG Li-jun, TONG Chuang-chuang, CAO Zhen. Structural stability and mechanical properties of Pt−Zr alloys from first-principles [J]. Journal of Alloys and Compounds, 2015, 643: 49−55.

[12] SAKURAI J, HATA S, YAMUCHI R, ABE M, SHIMOKOHBE A. Searching for Pt−Zr−Ni thin film amorphous alloys for optical glass lenses molding materials [J]. Precision Engineering-Journal of the International Societies for Precision Engineering and Nanotechnology, 2010, 34: 431−439.

[13] LIEBSCHER C H, GLATZEL U. Configuration of superdislocations in the γ'-Pt_3Al phase of a Pt-based superalloy [J]. Intermetallics, 2014, 48: 71−78.

[14] LIU Yan-jun, HUANG Hua-wei, PAN Yong, ZHAO Guang-hui, LIANG Zheng. First-principles study on the phase transition, elastic properties and electronic structure of Pt_3Al alloys under high pressure [J]. Journal of Alloys and Compounds, 2014, 597: 200−204.

[15] RAZUMOVSKIY V I, ISAEV E I, RUBAN A V, KORZHAVYI P A. Ab initio calculations of elastic properties of Pt−Sc alloys [J]. Intermetallics, 2008, 16: 982−986.

[16] KIM D E, MANGA V R, PRINS S N, LIU Z K. First-principles calculations and thermodynamic modeling of the Al−Pt binary system [J]. Calphad, 2011, 35: 20−29.

[17] ZHOU Yun-xuan, YU Wei, CHONG Xiao-yu, WEI Yan, HU Chang-yi, ZHANG Ai-min, FENG Jing. Rapid screening of alloy elements to improve the elastic properties of dilute Pt-based alloys: High-throughput first-principles calculations and modeling [J]. Journal of Applied Physics, 2020, 128: 235103.

[18] KIM D, SHANG Shun-li, LIU Zi-kui. Effects of alloying elements on thermal expansions of γ-Ni and γ'-Ni_3Al by first-principles calculations [J]. Acta Materialia, 2012, 60: 1846−1856.

[19] DAI Fu-zhi, FENG Zhi-hai, ZHOU Yan-chun. First principles investigation on mechanical and thermal properties of α- and β-$YAlB_4$ ultra-high temperature ceramics [J]. Journal of the American Ceramic Society, 2018, 101: 5694−5704.

[20] SHANG Shun-li, WANG Yi, KIM D, LIU Zi-kui. First-principles thermodynamics from phonon and Debye model: Application to Ni and Ni_3Al [J]. Computational Materials Science, 2010, 47: 1040−1048.

[21] TETER D M, GIBBS G V, BOISEN M B, ALLAN D C, TETER M P. First-principles study of several hypothetical silica framework structures [J]. Physical Review B, 1995, 52: 8064−8073.

[22] MORUZZI V L, JANAK J F, SCHWARZ K. Calculated thermal properties of metals [J]. Physical Review B, 1988, 37: 790−799.

[23] WANG Jie-min, WANG Jing-yang, ZHOU Yan-chun, HU Chun-feng. Phase stability, electronic structure and

mechanical properties of ternary-layered carbide Nb_4AlC_3: An ab initio study [J]. Acta Materialia, 2008, 56: 1511−1518.
[24] YU Wei, ZHOU Yun-xuan, CHONG Xiao-yu, WEI Yan, HU Chang-yi, ZHANG Ai-min, FENG Jing. Investigation on elastic properties and electronic structure of dilute Ir-based alloys by first-principles calculations [J]. Journal of Alloys and Compounds, 2021, 850: 156548.
[25] WANG Yi, LIAO Ming-qing, BOCKLUND B J, GAO Peng, SHANG Shun-li, KIM H, BEESE A M, CHEN LONG-qing, LIU Zi-kui. DFTTK: Density functional theory toolkit for high-throughput lattice dynamics calculations [J]. Calphad, 2021, 75: 102355(1−15).
[26] CHONG Xiao-yu, PALMA J P S, WANG Y, SHANG Shun-li, DRYMIOTIS F, RAVI V A, STAR K E, FLEURIAL J P, LIU Zi-kui. Thermodynamic properties of the Yb−Sb system predicted from first-principles calculations [J]. Acta Materialia, 2021, 217: 117169(1−12).
[27] PERDEW J P, WANG Yi. Accurate and simple analytic representation of the electron-gas correlation energy [J]. Physical Review B, 2018, 98: 13244−13249.
[28] TOGO A, TANAKA I. First principles phonon calculations in materials science [J]. Scripta Materialia, 2015, 108: 1−5.
[29] XIANG Shi-kai, CAI ling-cang, BI Yan, JING Fu-qian, WANG Shun-jin. Thermal equation of state for Pt [J]. Physical Review B, 2005, 72: 184102.
[30] KITTEL C, MASI J F. Introduction to solid state physics [J]. Physics Today, 1954, 7: 18−19.
[31] RAJU S, MOHANDAS E, RAGHUNATHAN V S. The pressure derivative of bulk modulus of transition metals: An estimation using the method of model potentials and a study of the systematics [J]. Journal of Physics and Chemistry of Solids, 1997, 58: 1367−1373.
[32] DUTTON D. H, BROCKHOUSE B N, MIILLER A P. Crystal dynamics of platinum by inelastic neutron scattering [J]. Canadian Journal of Physics, 1972, 50: 2915−2927.
[33] ARBLASTER J W. The thermodynamic properties of platinum [J]. Platinum Metals Review, 2005, 49: 141−149.
[34] BARIN I, PLATZKI G. Thermochemical data of pure substances [M]. 3rd ed. Weinheim: VCH, 2008.
[35] SEVILLE A H. The heat capacity of platinum at high temperatures [J]. The Journal of Chemical Thermodynamics, 1975, 7: 383−387.
[36] BERG W T. The low temperature heat capacity of platinum [J]. Journal of Physics and Chemistry of Solids, 1969, 30: 69−72.
[37] FURUKAWA G T, REILLY M L, GALLAGHER J S. Critical analysis of heat—capacity data and evaluation of thermodynamic properties of ruthenium, rhodium, palladium, iridium, and platinum from 0 to 300 K. A survey of the literature data on osmium [J]. Journal of Physical and Chemical Reference Data, 1974, 3: 163−209.
[38] YOKOKAWA H, TAKAHASHI Y. Laser-flash calorimetry II. Heat capacity of platinum from 80 to 1000 K and its revised thermodynamic functions [J]. The Journal of Chemical Thermodynamics, 1979, 11: 411−420.
[39] KIRBY R K. Platinum — A thermal-expansion reference material [J]. International Journal of Thermophysics, 1991, 12: 679−685.
[40] TOULOUKIAN Y S, BUYCO E H. Thermophysical properties of matter—The TPRC data series [R]. 1975.
[41] GRAYDE. American institute of physics handbook [M]. New York: McGraw-Hill, 1982.
[42] COLLARDSM, MCLELLAN R B. High-temperature elastic constants of platinum single crystals [J]. Acta Metallurgica et Materialia, 1991, 40: 699−702.
[43] DOROGOKUPETSPI, OGANOV A R. Ruby, metals, and MgO as alternative pressure scales: A semiempirical description of shock-wave, ultrasonic, X-ray, and thermochemical data at high temperatures and pressures [J]. Physical Review B, 2007, 75: 024115.

合金元素对 Pt 基合金热弹性性能的影响

余 威[1]，种晓宇[1]，千梦迪[1]，魏 燕[2]，张爱敏[2]，胡昌义[2]，冯 晶[1]

1. 昆明理工大学 材料科学与工程学院，昆明 650093；
2. 昆明贵研新材料科技有限公司，昆明 650106

摘 要：采用基于第一性原理计算的准静态近似方法，研究 33 种合金元素对 Pt 基合金热弹性性能的影响。研究表明：当稀土元素(Y、La、Ce 或 Th)固溶进入 Pt 基体后，由于稀土元素和 Pt 之间的平均键长较长，Pt 基合金 $Pt_{31}X$ 的弹性常数和弹性模量变小；与纯 Pt 相比，合金元素 Ta、Nb、V、W 或 Mo 固溶进入 Pt 基体后会产生强烈的电子局域化并使平均键长缩短，从而提高 Pt 基合金的杨氏模量；同时，由于 $Pt_{31}X$ (X=Ta，Nb，V，W 和 Mo)的平均键长随温度的升高缓慢增加，因此，其模量温度系数较小，其中，$Pt_{31}W$ 的模量温度系数最小($-15.82\times10^{-5}\ K^{-1}$)。因此，W、Ta、Mo、Nb 或 V 是潜在的具有增强 Pt 弹性稳定性的合金元素。

关键词：第一性原理计算；热学性质；弹性性质；准静态近似；Pt 基合金

(Edited by Wei-ping CHEN)